Available online at www.sciencedirect.com
ScienceDirect
Polymer 48 (2007) 2415–2424
polymer
www.elsevier.com/locate/polymer

Poly(trimethylene terephthalate) copolyester containing ethylene glycol moieties. Part 1: Crystallization kinetics and melting behavior

Chi-Yun Ko [a], Ming Chen [a,*], Chuan-Liang Wang [a], Hui-Chen Wang [a], Ren-Yi Chen [a], I-Min Tseng [b]

[a] *Institute of Materials Science and Engineering, National Sun Yat-Sen University, 70 Lien Hai Road, Kaohsiung 80424, Taiwan, ROC*
[b] *Union Chemical Laboratories, Industrial Technology Research Institute, Hsinchu 300, Taiwan, ROC*

Received 15 April 2005; received in revised form 9 January 2007; accepted 11 February 2007
Available online 20 February 2007

Abstract

A copolyester was characterized to have 91 mol% trimethylene terephthalate unit and 9 mol% ethylene terephthalate unit in a random sequence by using ^{13}C NMR. Differential scanning calorimeter (DSC) was used to investigate the isothermal crystallization kinetics in the temperature range (T_c) from 180 to 207 °C. The melting behavior after isothermal crystallization was studied by using DSC and temperature modulated DSC (TMDSC). The exothermic behavior in the DSC and TMDSC curves gives a direct evidence of recrystallization. No exothermic flow and fused double melting peaks at $T_c = 204$ °C support the mechanism of different morphologies. The Hoffman–Weeks linear plot gave an equilibrium melting temperature of 236.3 °C. The kinetic analysis of the growth rates of spherulites and the morphology change from regular to banded spherulites indicated that there existed a regime II → III transition at 196 °C.

Keywords: Copolyester; NMR; Crystallization

1. Introduction

Linearly polymerized esters of terephthalic acid and glycols have been synthesized by Whinfield and Dickson in 1941, and have been patented in 1946 and 1949 [1,2]. It is advantageous to use glycols having from 2 to 4 methylene groups, since these give highly polymerized esters with very high melting points. Poly(ethylene terephthalate) (PET) can crystallize over a wide temperature range between the glass transition temperature (T_g, 78 °C) and the melting temperature (T_m, 253 °C) [3]. The multiple melting behavior of PET and the origin of this phenomenon have been intensively studied [4–15]. However, PET has a slow rate of crystallization in molding [16,17] and cannot be molded neat with acceptable molding cycles. Poly(trimethylene terephthalate) (PTT) is also a aromatic polyester with a T_g of 44 °C and a T_m of 228 °C [3], and can be crystallized easily without adding nucleation agents [18,19]. For a long time, PTT did not find commercial interest due to the limited availability of 1,3-propanediol (3G), the monomer used for PTT synthesis. Recently, PTT has drawn attention because of Shell's break-through in lower-cost monomer processes [20]. Only limited information is available about its crystallization kinetics [21–26] and its multiple melting behavior of PTT [27–30]. Temperature modulated differential scanning calorimetry (TMDSC) is a thermal analysis technique [27,31–41], which could separate the total heat flow into the heat capacity-related (reversible) and kinetic (non-reversible) components. This makes TMDSC a powerful technique for the separation of exotherm from glass transition, reversible melting, or other heat capacity-related events.

Modifications of the chemical composition and the sequence distribution of semicrystalline polymers by copolymerization will alter both the crystallization kinetics and the morphology. Up to now, only a small number of works are

* Corresponding author. Tel.: +886 7 382 4680; fax: +886 7 525 4099.
E-mail address: mingchen@mail.nsysu.edu.tw (M. Chen).

0032-3861/$ - see front matter © 2007 Elsevier Ltd. All rights reserved.
doi:10.1016/j.polymer.2007.02.042

reported on poly(ethylene terephthalate-*co*-trimethylene terephthalate) (PET/PTT) copolyesters [3,42–49]. The composition of these copolyesters was determined only by proton nuclear magnetic resonance (^{1}H NMR) [42–47]. Lee et al. [45] synthesized a series of PET/PTT copolyesters by reacting dimethyl terephthalate (DMT), ethylene glycol (2G) and 3G in a two-step reaction sequence. Their thermal properties and non-isothermal crystallization kinetics were studied by differential scanning calorimetry (DSC). Wu and Lin [46] studied the isothermal crystallization kinetics and the melting behavior of PET/PTT copolyesters by DSC. These copolyesters were assumed to be random from the fact of a single T_g rather than two T_gs corresponding to possible blocks of PET and PTT [45,46]. In previous studies, Ko et al. [3] determined the compositions and the sequence distribution of 2G and 3G from the quaternary aromatic carbons of a series of PET/PTT copolyesters and presented the melting behavior of copolyesters after non-isothermal crystallization by using TMDSC.

The present study is one of the continuations of research on random copolyesters [3]. This paper is focused on the crystallization kinetics and the melting behavior of PT91/ET09 copolyester. ^{13}C NMR was used to determine the composition and the sequence distribution of this copolyester. Over a wide range of isothermal crystallization temperature (T_c), the DSC data were analyzed using the Avrami equation [50,51]. Linear growth rates of spherulites were measured in polarized light microscope (PLM) and the regime transition temperature was analyzed from the Lauritzen–Hoffman (LH) equation [52]. The morphology of this copolyester at various T_c was observed under PLM. In addition, the origin of multiple melting behaviors of isothermally crystallized specimens was elucidated using wide-angle X-ray diffraction (WAXD), DSC and TMDSC by varying the T_c, the crystallization time and/or the heating rate. In the second part of PT91/ET09 copolyester, the regime transitions of I → II and II → III will be reported and further discussed.

2. Experimental

2.1. Materials and characterization

Developmental grade PT91/ET09 copolyester was synthesized by three steps [3,53]. This copolyester had an intrinsic viscosity [η] of 0.84 dL/g measured in phenol/1,1,2,2-tetrachloroethane (3/2, w/w) at 25 ± 0.2 °C using an Ubbelohde viscometer. ^{1}H NMR spectroscopy was used to determine the composition of the copolyester. ^{13}C NMR analysis was performed for determining both the copolyester composition and the ester sequence distribution in the copolymer. The ^{13}C NMR and ^{1}H NMR spectra of $CF_3COOD/CDCl_3$ (4/1, v/v) solutions were recorded on the Bruker AMX-400 NMR spectrometer at 320 K. In order to have a quantitative response, the ^{13}C NMR spectra were determined by using a 20-s pulse cycle [3]. This condition ensured the complete relaxation of all the nuclei to be analyzed, therefore the relative peak areas could be measured in an automatic integration mode.

The copolyester pellets and the compressed sheets with a thickness of about 0.2 mm were dried at 45 °C in a vacuum oven for 12 h to remove moisture before using. Amorphous specimen, quenched from the melt, was used to obtain its T_g in a Perkin–Elmer Pyris 1 DSC at a heating rate of 1, 5 and 10 °C/min. The corresponding T_g at the zero heating rate is 42.1 °C (315.2 K).

2.2. Differential scanning calorimetry (DSC) and sample preparation

A Perkin–Elmer Pyris 1 DSC was used to investigate the isothermal crystallization kinetics and the melting behavior of the copolyester under nitrogen. Both temperature and heat flow scales were routinely calibrated with indium and zinc under a constant nitrogen flux. About 3–5 mg of sample was used in this study. Each sample was first heated up to 245 °C with 10 °C/min and dwelled for 5 min at the melt, followed by cooling to a chosen T_c between 180 and 207 °C with a most rapid rate. The samples were crystallized for 3–5 times of the peak time to ensure the completion of crystallization. After isothermal crystallization, the specimens were ready for DSC, TMDSC and WAXD studies. The exothermal curves of heat flow as a function of time were recorded and analyzed by Avrami's method [50,51]. To study the melting behavior, the samples were scanned up to 250 °C at 10 and 50 °C/min. To study the origin for the occurrence of the multiple melting peaks, the samples were treated in the same pre-melting condition except that the isothermal crystallization time was varied. Then they were scanned directly from T_c up to 230 °C at 50 °C/min.

2.3. Temperature modulated DSC (TMDSC)

A TA Q100 TMDSC equipped with a refrigerated cooling system was also used to investigate the melting behavior of the specimens after completely isothermal crystallization. Nitrogen gas was used as a purge gas and the flow rate was 50 ml/min. The cell constant calibration was performed with an indium standard, and the temperature calibration was obtained with indium and lead metals. A standard sapphire sample was used to measure the heat capacity calibration constant for the modulation study. The heating was operated at 2 °C/min with the modulation amplitude of 0.212 °C and the modulation period of 40 s, based on the recommended specifications given in the instrument manual [54]. The modulation amplitude was smaller relative to the heating rate, so there was no local cooling during the scan, which was referred to as heating-only.

2.4. Wide-angle X-ray diffraction

X-ray diffractograms at room temperature were acquired by a Siemens D5000 diffractometer using Ni-filtered Cu Kα radiation ($\lambda = 0.1542$ nm, 40 kV, 30 mA) at a scanning rate of 1°/min.

2.5. Polarized light microscopy (PLM)

The setups and the measurements for the experiments of polarized light microscopy are described in previous studies [55,56]. Specimens were prepared by melting the PTT/PET sample on a slide glass at 260 °C for 3 min to remove thermal history. The pre-molten specimens were quickly cooled to a preset temperature between 180 and 204 °C. Development of the spherulites was recorded as a function of time during the crystallization process. The sign of birefringence of the spherulite textures was determined by means of a primary red filter (λ-plate) located diagonally between cross polarizers.

3. Results and discussion

3.1. Copolyester composition and sequence distribution

^{13}C NMR spectrum of this copolyester is shown in Fig. 1a, where the assignment of each peak is based on the ^{13}C NMR results of PTT and PET homopolymers [57]. The ranges of carbon chemical shifts are 63.2–64.0, 62.5–63.0, and 27.8–28.1 ppm, respectively, for the ethylene carbons (label a) in the $-OCH_2CH_2O-$ unit and the methylene carbons α (label b) and β (label c) to the ester oxygen in the $-OCH_2CH_2CH_2O-$ unit. The chemical shifts of quaternary aromatic carbons (label d), aryl carbons (label e), and carbonyl carbons (label f) are 133.6–134.0, 129.6–130.2, and 165.9–168.2 ppm, respectively. The possibilities of three triads in this copolyester are *P*(ETE), *P*(PTP) and *P*(ETP) (where E represents ethylene glycol unit, T is terephthalate unit, and P denotes 1,3-propanediol unit). An enlarged ^{13}C NMR spectrum in the range of 133.3–134.2 ppm is shown in Fig. 1b, where four peaks are assigned to ETE (A, 133.7 ppm), PTP (B, 133.8 ppm), ETP-E side (C, 133.6 ppm), and ETP-P side (D, 133.9 ppm) triads, respectively [3]. This copolymer is characterized to have 91.1 mol% of trimethylene terephthalate (PT) unit, and 8.9 mol% of ethylene terephthalate (ET) unit. The composition was also determined from ^{1}H NMR integration of the center methylene in the 1,3-propanediol moiety at 2.3 ppm relative to the methylenes in the ethylene glycol moiety at 4.8 ppm [45]. The composition

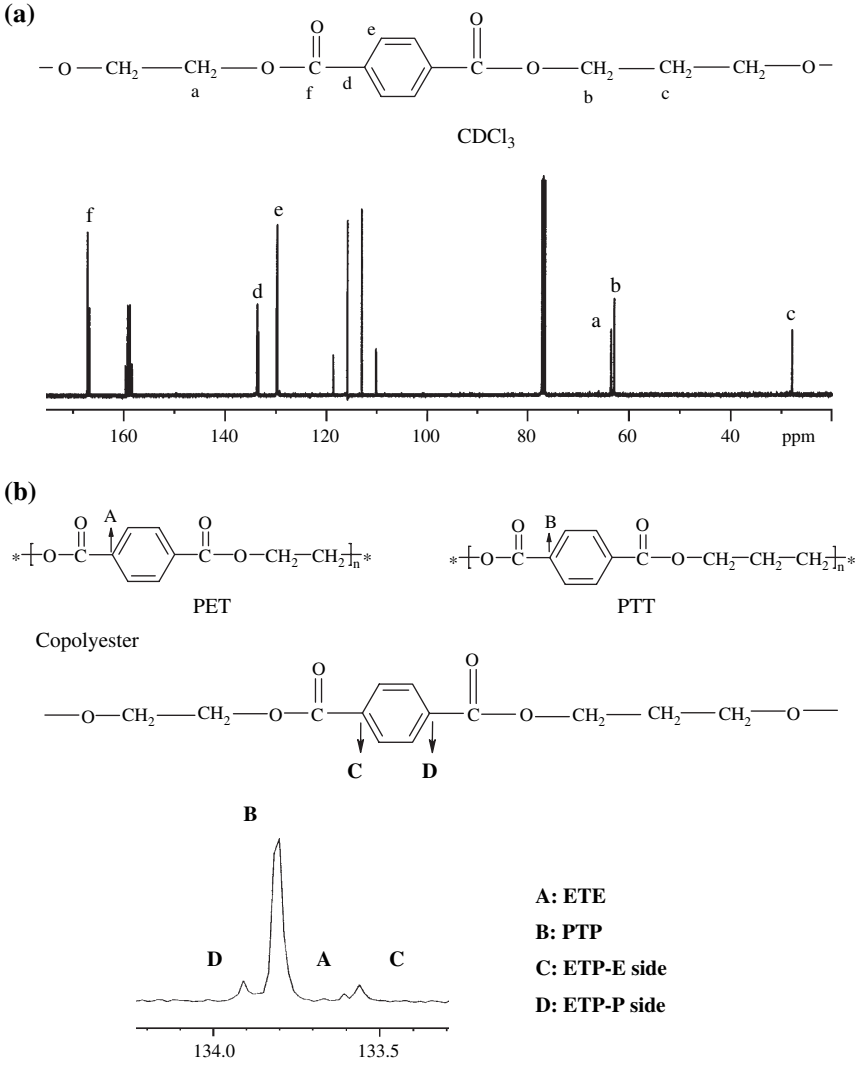

Fig. 1. (a) 100 MHz ^{13}C NMR spectrum and its peak assignment; (b) an enlarged spectrum in the range of quaternary aromatic carbons.

is 93.1 mol% of PT unit, which is very close to that observed in the ^{13}C NMR spectra. This copolyester was denoted as PT91/ET09 in the previous paper [3].

The randomness or irregularity factor B [58,59] is given by $P(ETP)/(2P_{PT} \times P_{ET})$, where P_{PT} and P_{ET} are the mole fraction of PT and ET units. The B value is 1.10 which is close to $B = 1.0$ for a random copolyester. The average number sequence lengths [58,60] for PT and ET units are 10.2 [$2P_{PT}/P(ETP)$, Ln_{PT}] and 1.0 [$2P_{ET}/P(ETP)$, Ln_{ET}], respectively. These results suggest that the sequence distribution of PT and ET units is statistically random for this copolyester.

3.2. Isothermal crystallization kinetics

The isothermal crystallization time, at temperatures ranging from 180 to 207 °C in an interval of 3 °C, is listed in the second column of Table 1. The required time (t_c) increased from 5 min at 180 °C to 163 min at 207 °C. The total enthalpy of crystallization (ΔH) and the half time of crystallization ($t_{1/2}$) are tabulated in columns 3 and 4 of Table 1. The average value of ΔH is -47 ± 2 J/g, and the individual ΔH is higher than that reported by Wu and Lin [46] at the same T_c. When $T_c = 180$ °C, the exothermic signal disappeared at about 2 min, and when $T_c = 207$ °C, the complete crystallization time was longer than 70 min. The values of $t_{1/2}$ increased with T_c, from 0.5 min at 180 °C to 24.8 min at 207 °C. The relative degree of crystallinity [$X_c(t)$] at time t was calculated. From the Avrami plot of $\log[-\ln(1 - X_c(t))]$ versus $\log t$, the Avrami exponents and rate constants, n_1 and k_1, are tabulated in the last two columns of Table 1. The n_1 values increased from 2.2 to 3.0 with an increasing T_c. This phenomenon can be explained as follows. First, the thickness of samples for DSC studies is about 0.2 mm. At higher T_cs, the nucleation density is low and the diameter of the spherulite is larger than 0.1 mm. Therefore, the growth of the spherulites was limited in two-dimensional space during the later stage of isothermal crystallization. Next, the homogeneous nucleation rate increases rapidly at low T_c. It represents an athermal nucleation process followed by three-dimensional crystal growth in the early stage of isothermal crystallization. Finally, the cooling rate of the coolant system is not fast enough to avoid crystallization of this copolyester before cooling to a lower T_c. As shown in Table 1, the values of k_1 decrease from 4.1×10^{-4} to 2.3×10^{-10} with an increasing T_c; in other words, it means that the overall rate constant decreases when the crystallization temperature increases.

Table 1
Summary of the condition and the kinetic analysis of crystallization for the specimens isothermally crystallized ranging from 180 to 207 °C

T_c (°C)	t_c (min)	ΔH (J/g)	$t_{1/2}$ (min)	n_1	k_1
180	5	−46.2	0.5	2.23	4.14×10^{-4}
183	7	−43.3	0.6	2.36	1.30×10^{-4}
186	9	−46.7	0.9	2.56	2.46×10^{-5}
189	12	−47.6	1.3	2.58	9.06×10^{-6}
192	15	−50.9	1.9	2.66	2.53×10^{-6}
195	18	−48.5	2.8	2.72	6.13×10^{-7}
198	27	−47.1	4.5	2.97	4.01×10^{-8}
201	42	−44.7	7.5	2.96	8.28×10^{-9}
204	78	−45.9	12.5	2.98	1.82×10^{-9}
207	163	−45.7	24.8	2.98	2.28×10^{-10}

3.3. Wide-angle X-ray diffraction

Fig. 2 shows the WAXD patterns of PT91/ET09 copolyester melt-crystallized isothermally at various temperatures. All of the patterns have the same diffraction peaks as PTT homopolymer with a triclinic unit cell [30,61–65]. The characteristic peaks at $2\theta \approx 15.6°$, 17.2°, 19.5°, 21.8°, 23.7°, and 24.9° were assigned to (010), $(0\bar{1}2)$, (012), (100), $(102, 10\bar{3})$, and $(1\bar{1}3)$ planes, respectively [61–65]. Therefore, there is only one form of crystal for the samples crystallized isothermally between 180 and 207 °C. The possibility of different crystal structures is excluded for this study. The multiple melting peaks should be due to the melting of different populations of lamellar crystals and/or the melting–recrystallization–remelting processes.

3.4. Melting behavior and mechanism of multiple melting peaks studied by conventional DSC

The DSC thermograms at a heating rate of 50 °C/min for specimens isothermally crystallized at 195 and 204 °C for different time durations are plotted in Fig. 3. In Fig. 3a, double melting peaks are shown for specimens crystallized at 195 °C isothermally up to 5.5 min. In Fig. 3b, single endothermic melting peak is shown for specimens crystallized at 204 °C isothermally up to 40 min. A lower melting peak at ~10 °C above T_c is not detected for T_cs at 195 and 204 °C, even the isothermal time is more than double of $t_{1/2}$. The peak intensities of all the peaks increase as the crystallization time increases, but the peak locations of the melting peaks remain constant over the range of crystallization time examined. The fact that the constant intensity ratio of two peaks in

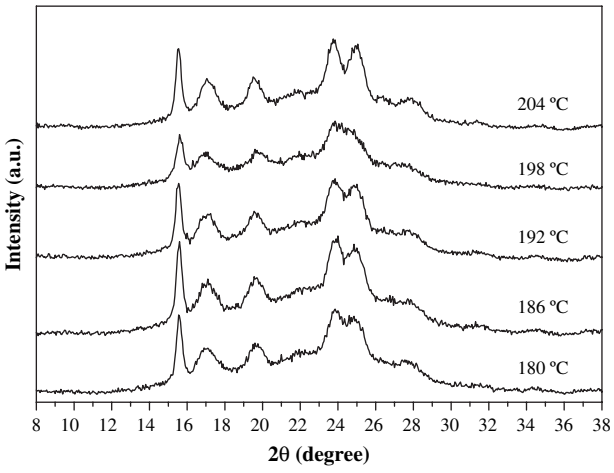

Fig. 2. X-ray diffraction patterns of the specimens isothermally crystallized at various temperatures.

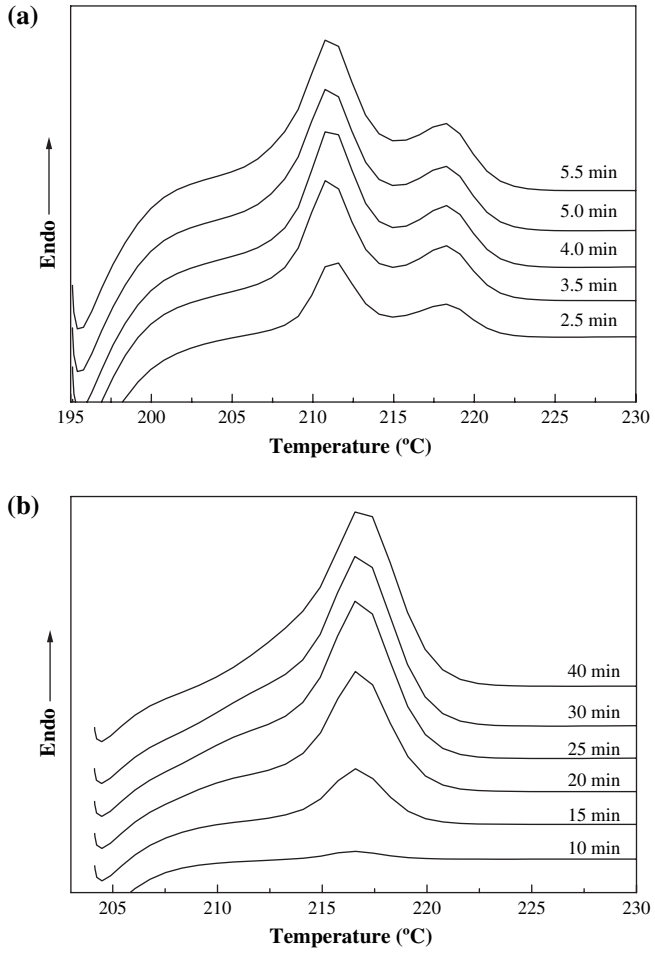

Fig. 3. DSC thermograms at a heating rate of 50 °C/min for the specimens after melting at 245 °C for 5 min, and then crystallized isothermally at (a) 195, (b) 204 °C for various time.

Fig. 3a and only one crystal structure regardless of T_c in Fig. 2 can be explained in two ways. First, these two peaks represent two populations of lamellae that grow simultaneously. However, it is hard to explain the phenomenon of single peak in Fig. 3b. The second possibility is the application of melt-recrystallization theory. The original crystallite formed at T_c (195 °C) started to melt above T_c, and part of the melt recrystallized and remelted in the temperature range from 215 to 222 °C with a peak temperature around 218 °C as in Fig. 3a. As T_c increases from 195 to 204 °C, less time is allowed to recrystallize during the heating scan at a rate of 50 °C/min and the growth rates of crystallites reduce to half (see the following section). It indicates that the contribution of recrystallization decreases and the melting peaks of original (or primary) and recrystallized crystallites may merge together. The melting endotherms in Fig. 3 can be explained by the recrystallization phenomenon.

Figs. 4 and 5 show the DSC thermograms at heating rates of 10 and 50 °C/min, respectively, for the specimens after completion of isothermal crystallization at the indicated T_c. In Fig. 5, a small endothermic signal at 60–70 °C is the T_g of semicrystalline specimens. The results of ^{13}C NMR analysis

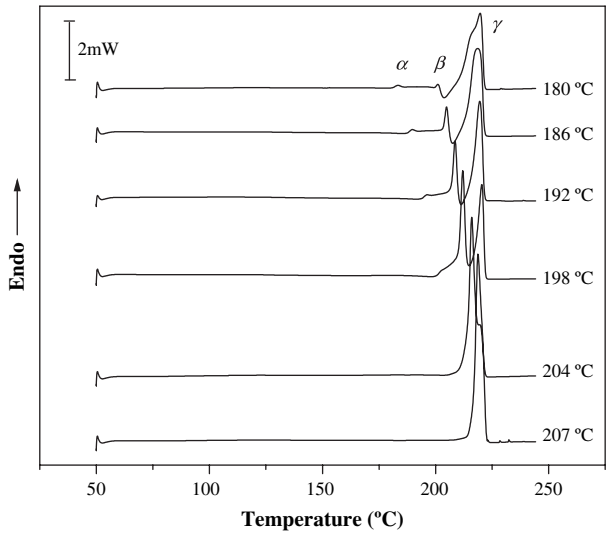

Fig. 4. DSC thermograms at a heating rate of 10 °C/min for the specimens isothermally melt-crystallized at the indicated temperatures.

and single T_g suggest that the sequence distribution of PT and ET units is statistically random for this copolyester. At $T_c \leq 192$ °C, three distinct endothermic peaks are observed in both figures, and a small exothermic peak can be detected between two endothermic peaks located at the high temperatures in Fig. 4. A little exothermic peak is also detected at $T_c = 180$ °C in Fig. 5. This phenomenon indicates that during the heating scan, recrystallization is much easier in the specimens crystallized under higher supercooling and heated at a lower rate. The endothermic peaks are labeled with Greek letters α, β and γ with increasing temperature in both figures. The peak temperatures of the melting peaks after deconvolution are tabulated in Table 2 for heating rates of 10 °C/min (columns 2–4) and 50 °C/min (columns 5–7), and are denoted as T_α, T_β and T_γ. T_α is 3–4 °C above T_c at 10 °C/min, and 7 ± 1 °C above T_c at 50 °C/min. Peak α shifts to the high temperature region as T_c increases, and its intensity is

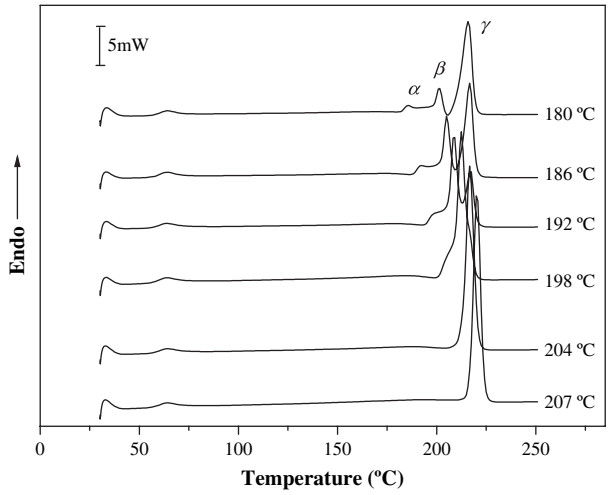

Fig. 5. DSC thermograms at a heating rate of 50 °C/min for the specimens isothermally melt-crystallized at the indicated temperatures.

Table 2
Melting peak temperatures at heating rates of 10 and 50 °C/min, respectively. All temperatures are in °C

T_c	T_{peak} at 10 °C/min			T_{peak} at 50 °C/min		
	T_α	T_β	T_γ	T_α	T_β	T_γ
180	183.4	(201.1)	219.7	185.7	201.6	215.8
183	186.5	(203.1)	219.6	189.0	203.2	215.8
186	189.7	204.9	218.9	192.4	204.9	216.6
189	192.9	206.7	218.9	195.7	206.6	216.6
192	196.0	208.7	219.6	199.1	209.1	216.6
195	199.2	210.4	220.1	202.4	210.7	216.6
198	–	212.1	220.6	205.8	212.4	216.6
201	–	214.1	220.6	–	214.1	–
204	–	216.1	219.9	–	216.6	–
207	–	218.7	–	–	219.9	–

relatively small that is associated with secondary crystallization. Peak β shifts to higher temperatures and increases in intensity as T_c increases, it is attributed to the fusion of the crystals grown during primary crystallization. The position of peak γ varies very little with T_c, however, its intensity decreases with increasing T_c. These results indicate that part of peak γ is due to the melting of the crystals recrystallized during the subsequent heating run after crystallized at a chosen T_c.

In the case of 10 °C/min, triple-melting peaks are detected at $T_c \leq 195$ °C and a single melting peak with a shoulder at high temperature side is observed at $T_c = 204$ °C (see Fig. 4 and Table 2). When the specimen is heated at 50 °C/min, triple-melting peaks are detected at $T_c \leq 198$ °C (see Fig. 5 and Table 2). Peak β and peak γ merge together to form a fused peak at $T_c = 204$ °C. Finally, peak β and peak γ merge completely to become a single peak at $T_c = 207$ °C, as shown in Fig. 5. Comparing the peak temperatures at the same T_c in Table 2, T_α and T_β at 50 °C/min are higher than those at 10 °C/min. This may be due to the superheating of polymer at a higher heating rate. However, the maximum temperature rise for peak β (or primary peak) is only 0.5 °C for $T_c \leq 204$ °C. In addition, T_β at $T_c = 180$ and 183 °C for heating rate of 10 °C/min is not accurate because it is a superposition of melting of primary crystals with almost simultaneous exothermic recrystallization. T_γs at 50 °C/min are less than those at 10 °C/min because a longer heating period at 10 °C/min allows the specimens to be recrystallized and/or reorganized during the heating scan. These results suggest that T_β measured at 50 °C/min is a better way to estimate the equilibrium melting temperature, T_m^o, without the superposition problem between the primary melting peak and the recrystallization exothermic peak. Therefore, the peak temperature of primary crystals measured at a heating rate of 50 °C/min (column 6 of Table 2) is designated as T_m. In order to determine T_m^o, T_m is plotted versus T_c in Fig. 6. A solid line is drawn where $T_c = T_m$. According to the Hoffman–Weeks method [66], the experimental data are extrapolated (dotted line made from the linear regression of the data points of filled squares with T_c ranging from 180 to 204 °C and a correlation coefficient of 0.9988) to the intersection with the solid line.

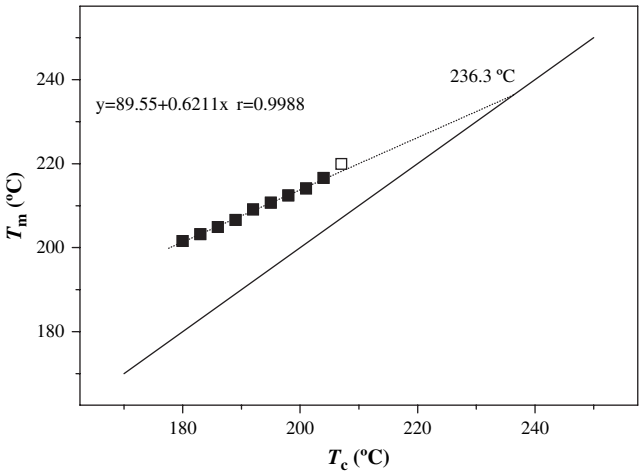

Fig. 6. Hoffman–Weeks plot for determining the equilibrium melting temperature of the copolyester from the conventional DSC data at a heating rate of 50 °C/min.

The temperature of intersection is T_m^o, which yields a value of 236.3 °C for this copolyester. Wu and Lin [46] presented that the T_m^o was 231.5 °C when the PET/PTT copolyester containing 91.4 mol% PT unit with T_c ranging from 180 to 195 °C was heated at 10 °C/min.

3.5. Melting behavior and mechanism of multiple melting peaks studied by TMDSC

Fig. 7 shows multiple peaks in the total curves of TMDSC traces. An enlarged curve for the melting peak P_α at $T_c = 180$ °C is inserted in the upper left corner. The melting peaks are labeled as P_α, $P_{\beta,endo}$, $P_{\beta',endo}$ and P_γ with increasing temperature in the figure, and denoted as T_α, $T_{\beta endo}$, $T_{\beta' endo}$ and T_γ. One exothermic peak is labeled as $P_{\beta,exo}$ with a peak temperature at $T_{\beta exo}$. This peak appears just prior to $P_{\beta',endo}$ for $T_c \leq 195$ °C and/or immediately after $P_{\beta,endo}$ for

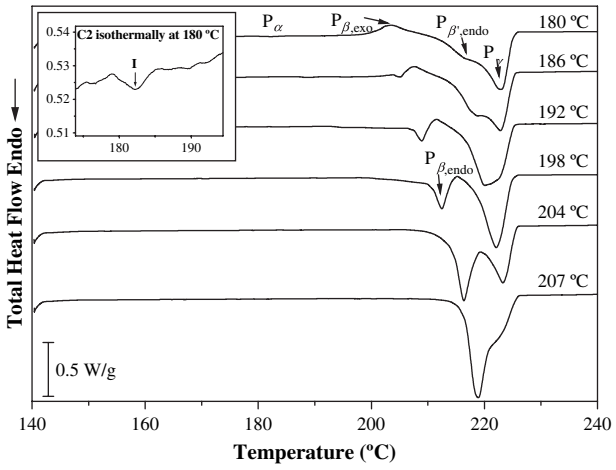

Fig. 7. Total heat flow of the TMDSC thermograms at a heating rate of 2 °C/min for the specimens isothermally melt-crystallized at the indicated temperatures.

$T_c \geq 186$ °C. P_α is very small and shifts to the high temperature region as T_c increases. T_α is only about 2–4 °C above T_c. $P_{\beta,endo}$ shifts to higher temperature and increases in intensity as T_c increases. It becomes a major peak for $T_c \geq 204$ °C. As T_c increases, a complicated melting behavior in the high temperature side is described as follows: (a) the position of P_γ (or T_γ) varies very little; (b) $P_{\beta',endo}$ appears as a shoulder of P_γ at $T_c = 180$ °C and increases in intensity; (c) the apparent $T_{\beta'endo}$ increases; (d) the relative intensity ratio of $P_{\beta',endo}/P_\gamma$ increases and merges into a single peak; (e) this single peak decreases in intensity and becomes as a shoulder of $P_{\beta,endo}$. The total enthalpies of multiple peaks (ΔH_{total}) are summed. Its value increased from 47 to 57 J/g as T_c increased. The exothermic enthalpy from the total curve ($\Delta H_{exo\text{-}total}$) decreases from −5.8 to −0.3 J/g as T_c increases from 180 to 195 °C and is zero for $T_c \geq 198$ °C.

The exothermic enthalpy ($\Delta H_{exo\text{-}total}$) gives a direct evidence of the model of melting–recrystallization–remelting behavior of PT91/ET09 copolyester. As T_c decreases, the melting temperature of the secondary crystals also decreases, and more time is allowed to recrystallize during the heating scan at a rate of 2 °C/min. It can be assumed that the crystallization exotherm is also not detected at $T_c \geq 204$ °C in Figs. 4 and 5 because less time is available for the recrystallization during the heating at a rate of 10 or 50 °C/min. However, a distinct shoulder located at T_γ is observed at $T_c = 204$ °C in Fig. 4. No exothermic flow and fused double melting peaks support the mechanism of different populations of lamellar crystals for the specimens isothermally crystallized at $T_c = 204$ °C. These results indicate that the complex melting behavior of this copolyester is due to both mechanisms of melting–recrystallization–remelting and different morphologies. As T_c increases, the contribution of melting–recrystallization–remelting process to the upper melting peak gradually decreased, and finally disappeared.

One additional endotherm was reported by Wu and Lin [46] for PTT and PET/PTT copolyester containing 91.4 mol% PT using conventional DSC. This phenomenon was observed only when these two polyesters were crystallized at lower T_cs and it was explained as the fusion of recrystallized crystallites with different stabilities. This additional endotherm was reported in the non-isothermal study of PT91/ET09 copolyester and other PT enriched PET/PTT copolyesters [3]. In this study, two peaks in the high temperature side are due to different lamellar thickness or due to remelting of the recrystallized crystals formed during the heating scan at a rate of 2 °C/min. From the comparison of PT91/ET09 in this study with poly(ether ether ketone) (PEEK) [41], PET and poly(ethylene naphthalate) (PEN) in the literatures [13,14,37,39], the melting peak of perfect crystals by the reorganization process appeared behind the melting peak of primary crystals (i.e., double melting peaks in the high temperature side) for PET and PEN samples [39] in the reversing curves, however, both melting peaks always merge together to form one single melting peak for PEEK samples [41]. This is due to the fact that the upper melting peak for PEEK sample was mainly attributed to the primary crystal, while that for PET and PEN samples were dominated by the perfect crystal due to the reorganization process.

3.6. Kinetic analysis of the growth rates of spherulites

By measuring the spherulitic radii from PLM micrographs taken at successive intervals during the isothermal crystallization, the growth rate (G) was determined by a linear least squares fit of the initial linear portion of the growth rate curves before impingement [53,54]. Fig. 8 plots the temperature dependence of the growth rate for the specimen after equilibration at 260 °C for 3 min. The growth rates range from 6.14×10^{-1} μm/s at 180 °C to 6.10×10^{-2} μm/s at 207 °C. The error bar is also plotted in Fig. 8 for each data point (or T_c). As expected, this confirms the decrease of the radial growth rate with increasing T_c in this temperature range. The measurable maximum growth rate of this copolyester is about one-third of the measurable maximum growth rate of PTT homopolymer [18,19]. High rates of nucleation and growth resulted in a high recrystallization rate of this PT91/ET09 copolyester.

Let us follow the regime analyses of the LH model [50] to treat our fitted growth rate data shown in Fig. 8. Fig. 9 shows a plot of $\log G + U^*/[2.303R(T_c - T_g + 30)]$ versus $1/(T_c \Delta T f)$ [52,55,56], which can provide the value of K_g (slope × 2.303) and $\log G_o$ (intercept) for each regime. G_o is the preexponential factor. U^* and T_∞ denote the WLF (Williams–Landel–Ferry) energy term and WLF temperature, respectively, $\Delta T = (T_m^o - T_c)$ is the undercooling, and f represents a correction term of the order of unity, which is normally expressed as

$$f = 2T_c/\left(T_m^o + T_c\right) \tag{1}$$

The regime analysis of the LH model was performed by using the following values: $U^* = 1500$ cal/mol, and $T_\infty = T_g - 30$ K with the T_g at 285.2 K. The value of $T_m^o = 236.3$ °C = 509.4 K was employed. The optimal fit with two lines is reflected in the correlation coefficients (0.9979 and 0.9999), as shown in Fig. 9. In this case, the growth rate data from 180 to 195 °C are plotted with filled triangles and used to fit a linear

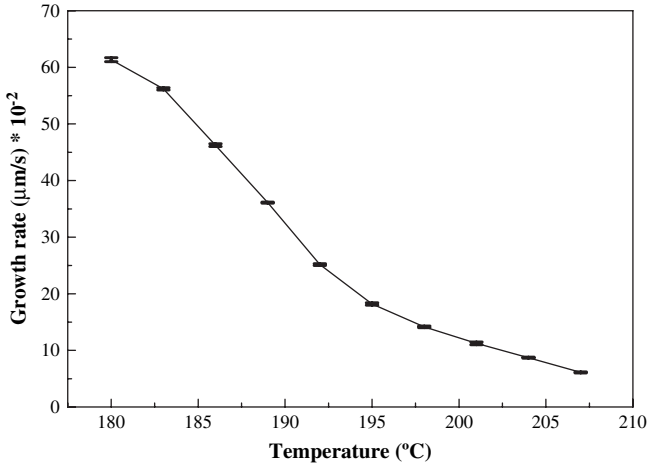

Fig. 8. Variation of spherulitic growth rates with temperature.

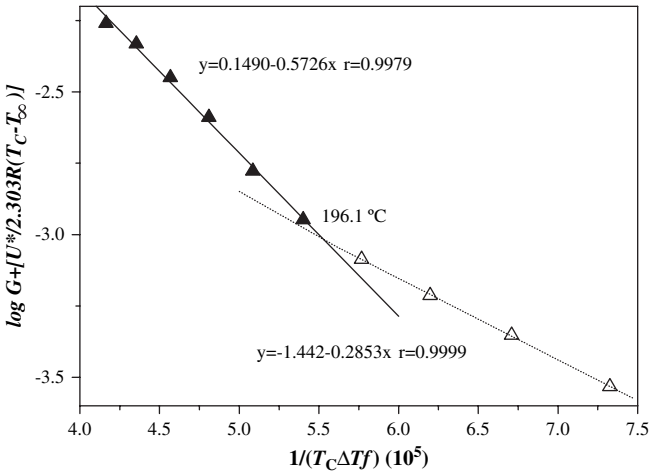

Fig. 9. The kinetic analysis of the growth rate data of spherulites. In this case, $U^* = 1500$ cal/mol, $T_\infty = T_g - 30\ \mathrm{K} = 285.2\ \mathrm{K}$ and $T_m^o = 509.4\ \mathrm{K}$, and the growth rate data from 180 to 195 °C (filled triangles) are used to fit a linear line in the higher undercooling region.

line in the higher undercooling region. The break in the curve occurs at $T_c = 196.1$ °C and the ratio of the two slopes is 2.01. Obviously, an attempt to put one straight line through all the data would lead to an inadmissible fit. Our results have thus demonstrated that this sample exhibits a regime II → III transition at 196 °C.

The appearance of the samples, crystallized from the melt at different T_cs, between crossed polaroids is shown in Figs. 10 and 11. These melt-crystallized thin films with free surface formed well-developed, two-dimensional spherulites with negative birefringence. They revealed a dark Maltese cross along the vibrational directions of polarizer and analyzer. In addition to these usual observations for polymeric materials, a system of dark concentric rings could be seen while the samples were crystallized at higher T_c ranging from 197 to 204 °C (Fig. 11). These observed ringed images are similar to the morphology of banded spherulite, which is generally observed in certain polymeric materials. At lower T_c (180, 189, 195, and 196 °C as shown in Fig. 10a–d), the banded morphology disappeared and exhibited regular spherulitic image. A clear change in morphology (from 196 to 197 °C) was detected based on PLM observation. This temperature is very close to the regime II → III transition at 196.1 °C, as determined from the kinetic analysis of the growth rates. Wu and Lin [46] also measured the growth rates of spherulites for the PET/PTT copolyester containing 91.4 mol% PT unit. The regime transition was not found because only six data ranging from 180 to 195 °C were used to do the kinetic analysis in that study. T_m^o, determined from the non-linear extrapolation of the Marand–Xu plot, and the effect of T_m^o values on the regime transition temperature will be reported in the next manuscript.

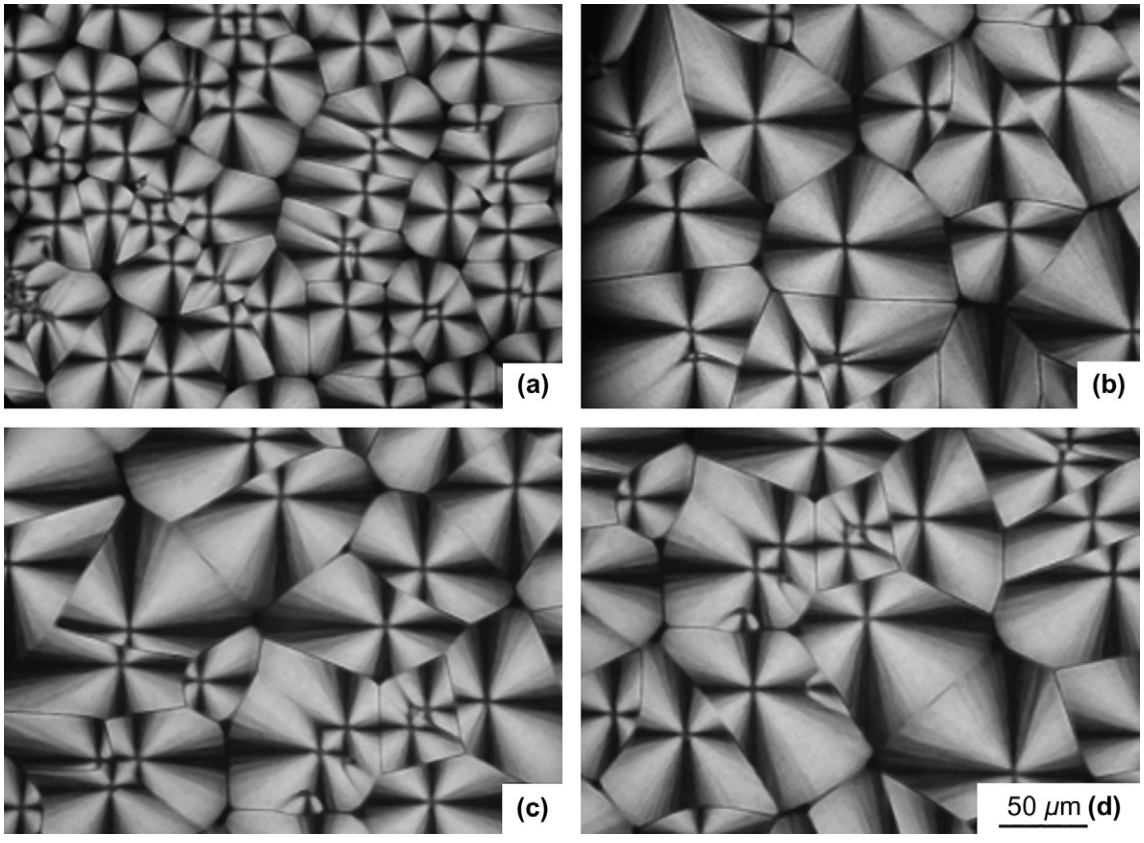

Fig. 10. Transmitted PLM micrographs with regular spherulites for the specimens melt-crystallized at the indicated temperatures: (a) 180, (b) 189, (c) 195, and (d) 196 °C.

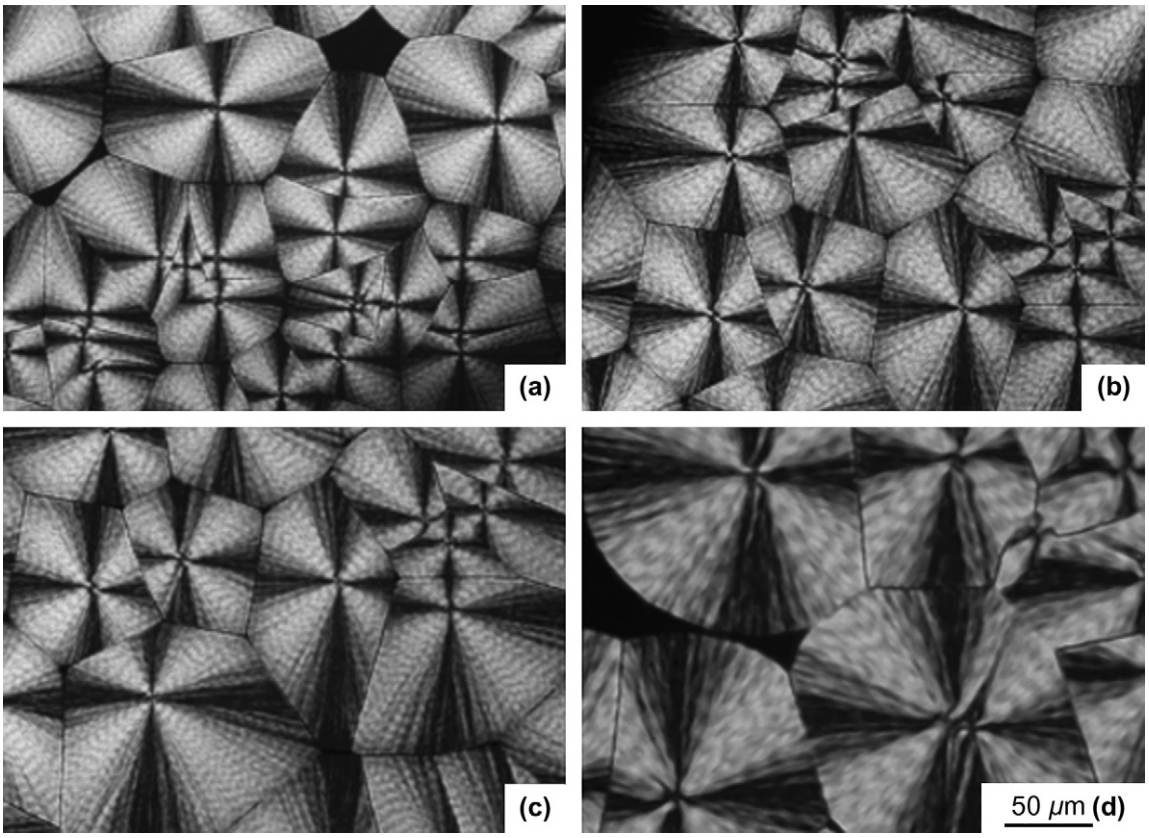

Fig. 11. Transmitted PLM micrographs with banded spherulites for the specimens melt-crystallized at the indicated temperatures: (a) 197, (b) 198, (c) 201, and (d) 204 °C.

4. Conclusion

The composition of this PET/PTT copolyester was found to have 91.1 mol% trimethylene terephthalate (PT) unit and 8.9 mol% ethylene terephthalate (ET) unit. The value of the random parameter, 1.10, is close to 1 for a random copolymer. In addition, a single T_g also suggests that this copolymer is a random copolyester. The average number sequence lengths for PT and ET units are 10.2 and 1.0, respectively. Single ET unit is distributed randomly along the polymer chain. The WAXD patterns suggest that there is only one crystal structure formed isothermally between 180 and 207 °C. Triple-melting peaks were found in the conventional DSC and TMDSC. The results indicate that the complex melting behavior of this copolyester is due to both mechanisms of melting–recrystallization–remelting and different morphologies. As the isothermal crystallization temperature increases, the contribution of melting–recrystallization–remelting process to the upper melting peak gradually decreased, and finally disappeared.

From the isothermal crystallization study, the n_1 values of Avrami exponent increased from 2.2 to 3.0 with an increasing T_c. The Hoffman–Weeks linear plot gave an equilibrium melting temperature of 193.6 °C. From the kinetic analysis by using the growth rates of the spherulites, there existed a regime II → III transition at 196.1 °C. A clear change in morphology from regular negative spherulites to banded negative spherulites was also observed at 196 °C based on the PLM micrographs. This temperature is consistent with the regime II → III transition determined from the kinetic analysis.

Acknowledgements

The authors acknowledge the financial support of the National Science Council of Taiwan, ROC, through Grants NSC 90-2216-E-110-014 and 91-2216-E-110-010.

References

[1] Whinfield JR, Dickson JT. Br Patent 578,079; June 14, 1946.
[2] Whinfield JR, Dickson JT. US Patent 2,465,319; March 22, 1949.
[3] Ko CY, Chen M, Wang HC, Tseng IM. Polymer 2005;46:8572.
[4] Roberts RC. Polymer 1969;10:117.
[5] Roberts RC. J Polym Sci Part B Polym Lett 1970;8:381.
[6] Nealy DL, Davis TG, Kibler CJ. J Polym Sci A-2 1970;8:2141.
[7] Holdsworth PJ, Turner-Jones A. Polymer 1971;12:195.
[8] Groeninckx G, Reynaers H. J Polym Sci Polym Phys Ed 1980;18:1325.
[9] Medellín-Rodríguez FJ, Phillips PJ. Macromolecules 1996;29:7491.
[10] Medellín-Rodríguez FJ, Phillips PJ, Lin JS, Campos R. J Polym Sci Part B Polym Phys 1997;35:1757.
[11] Qiu G, Tang ZL, Huang NX, Gerking L. J Appl Polym Sci 1998;69:729.
[12] Zhou C, Clough SB. Polym Eng Sci 1988;28:65.
[13] Wang ZG, Hsiao BS, Sauer BB, Kampert WG. Polymer 1999;40:4615.
[14] Wang Y, Lu J, Shen D. Polym J 2000;32:560.
[15] Kong Y, Hay JN. Polymer 2003;44:623.

[16] Wunderlich B. Macromolecular physics, vol. 2. New York: Academic Press; 1976. p. 163.
[17] Jog JP. J Macromol Sci Rev Macromol Chem Phys 1995;C35:531.
[18] Chen CC, Chen M, Tseng IM. J Macromol Sci Phys 2002;B41:1043.
[19] Chen M, Chen CC, Ke KZ, Ho RM. J Macromol Sci Phys 2002; B41:1063.
[20] Brown HS, Chuah HH. Chem Fiber Int 1997;47:72.
[21] Lee KM, Kim KJ, Kim YH. Polymer (Korea) 1999;23:56 [in Korea].
[22] Huang JM, Chang FC. J Polym Sci Part B Polym Phys 2000;38:934.
[23] Chisholm BJ, Zimmer JG. J Appl Polym Sci 2000;76:1296.
[24] Chuah HH. Polym Eng Sci 2001;41:308.
[25] Wang XS, Yan D, Tian GH, Li XG. Polym Eng Sci 2001;41:1655.
[26] Hong PD, Chung WT, Hsu CF. Polymer 2002;43:3335.
[27] Pyda M, Wunderlich B. J Polym Sci Part B Polym Phys 2000;38:622.
[28] Chung WT, Yeh WJ, Hong PD. J Appl Polym Sci 2002;83:2426.
[29] Wu PL, Woo EM. J Polym Sci Part B Polym Phys 2003;41:80.
[30] Srimoaon P, Dangseeyun N, Supaphol P. Eur Polym J 2004;40:599.
[31] Reading M. Trends Polym Sci 1993;8:248.
[32] Reading M, Elliott D, Hill VL. J Therm Anal 1993;40:949.
[33] Reading M, Luget A, Wilson R. Thermochim Acta 1994;238:295.
[34] Okazaki I, Wunderlich B. Macromol Rapid Commun 1997;18:313.
[35] Okazaki I, Wunderlich B. Macromolecules 1997;30:1758.
[36] Wurm A, Merzlyakov M, Schick C. J Macromol Sci Phys 1999;B38:693.
[37] Sauer BB, Kampert WG, Neal Blanchard E, Threefoot SA, Hsiao BS. Polymer 2000;41:1099.
[38] Kampert WG, Sauer BB. Polym Eng Sci 2001;41:1714.
[39] Kampert WG, Sauer BB. Polymer 2001;42:8703.
[40] Wunderlich B. Prog Polym Sci 2003;28:383.
[41] Wei CL, Chen M, Yu FE. Polymer 2003;44:8185.
[42] Smith JG, Kibler CJ, Sublett BJ. J Polym Sci Part A-1 Polym Chem 1966;4:1851.
[43] Ponnusamy E, Balakrishnan T. J Macromol Sci Chem 1985;A22:373.
[44] Ponnusamy E, Balakrishnan T. Polym J 1985;17:473.
[45] Lee JW, Lee SW, Lee B, Ree M. Macromol Chem Phys 2001;202:3072.
[46] Wu TM, Lin YW. J Polym Sci Part B Polym Phys 2004;42:4255.
[47] Wei GF, Wang LY, Chen GK, Gu LX. J Appl Polym Sci 2006;100:1511.
[48] Shyr TW, Lo CM, Ye SR. Polymer 2005;46:5284.
[49] Kiyotsukuri T, Masuda T, Tsutsumi N. Polymer 1994;35:1274.
[50] Avrami M. J Chem Phys 1939;8:212.
[51] Avrami M. J Chem Phys 1941;9:177.
[52] Hoffman JD, Davis GT, Lauritzen Jr JI. In: Hannay NB, editor. Treatise on solid state chemistry, vol. 3. New York: Plenum Press; 1976 [chapter 7].
[53] Tseng IM, Kuo TY, Shu WC, Huang JC. US Patent 6,187,900; February 13, 2001.
[54] TA Instruments. DSC 2910 differential scanning calorimeter, Operator's manual, Rev. 8. New Castle, Delaware; 1997. p. C-73.
[55] Chen M, Chung CT. J Polym Sci Part B Polym Phys 1998;36:2393.
[56] Chen JY, Chen M, Chao SC. Macromol Chem Phys 1998;199:1623.
[57] Chen M, Wang HC, Ko CY. Abstr Pap Am Chem Soc August 18 2002;224:166. Poly Part 2.
[58] Newmark RA. J Polym Sci Polym Chem Ed 1980;18:559.
[59] Yamadera R, Murano M. J Polym Sci A-1 Polym Chem 1967;5:2259.
[60] Backson SCE, Kenwright AM, Richards RW. Polymer 1995;36:1991.
[61] Ho RM, Ke KZ, Chen M. Macromolecules 2000;33:7529.
[62] Wang B, Li CY, Hanzlicek J, Cheng SZD, Geil PH, Grebowicz J, et al. Polymer 2001;42:7171.
[63] Poulin-Dandurand S, Pérez S, Revol JF, Brisse F. Polymer 1979;20:419.
[64] Moss B, Dorset DL. J Polym Sci Polym Phys Ed 1982;20:1789.
[65] Dorset DL, Moss B. Polymer characterization. Washington, DC: American Chemical Society; 1983. p. 409 [chapter 22].
[66] Hoffman JD, Weeks JJ. J Res Natl Bur Stand 1962;66A:13.